University of Reading

Ecosystem photosynthesis in land-surface models: a first-principles approach incorporating acclimation

Article

Published Version

Creative Commons: Attribution 4.0 (CC-BY)

Open Access

Mengoli, G., Agustí-Panareda, A., Boussetta, S., Harrison, S. P. ORCID: https://orcid.org/0000-0001-5687-1903, Trotta, C. and Prentice, I. C. (2022) Ecosystem photosynthesis in land-surface models: a first-principles approach incorporating acclimation. Journal of Advances in Modeling Earth Systems, 14 (1). e2021MS002767. ISSN 1942-2466 doi: 10.1029/2021MS002767 Available at https://centaur.reading.ac.uk/117392/

It is advisable to refer to the publisher's version if you intend to cite from the work. See Guidance on citing.

To link to this article DOI: http://dx.doi.org/10.1029/2021MS002767

Publisher: American Geophysical Union

All outputs in CentAUR are protected by Intellectual Property Rights law, including copyright law. Copyright and IPR is retained by the creators or other copyright holders. Terms and conditions for use of this material are defined in the End User Agreement.

University of Reading

www.reading.ac.uk/centaur

CentAUR

Central Archive at the University of Reading

Reading's research outputs online

Check for updates

JAMES | Journal of Advances in Modeling Earth Systems

RESEARCH ARTICLE
10.1029/2021MS002767

Ecosystem Photosynthesis in Land-Surface Models: A First-Principles Approach Incorporating Acclimation

Giulia Mengoli[1], Anna Agustí-Panareda[2], Souhail Boussetta[2], Sandy P. Harrison[3], Carlo Trotta[4], and I. Colin Prentice[1,5,6]

[1]Department of Life Sciences, Georgina Mace Centre for the Living Planet, Imperial College London, Silwood Park Campus, Ascot, UK, [2]European Centre for Medium Range Weather Forecasts, Reading, UK, [3]Geography & Environmental Sciences, Reading University, Whiteknights, Reading, UK, [4]Division on Impacts on Agriculture, Forests and Ecosystem Services (IAFES), Fondazione Centro Euro-Mediterraneo sui Cambiamenti Climatici (CMCC), Viterbo, Italy, [5]Department of Biological Sciences, Macquarie University, North Ryde, NSW, Australia, [6]Department of Earth System Science, Tsinghua University, Beijing, China

Key Points:

- Optimality theory is used to develop a model incorporating fast and acclimated responses of photosynthesis and stomatal conductance
- Biogeochemical photosynthetic capacities adjust to midday light conditions
- The new parameter-sparse model simulates gross primary production on sub-daily timesteps across a range of vegetation types and climates

Supporting Information:

Supporting Information may be found in the online version of this article.

Correspondence to:

G. Mengoli,
gmengoli@ic.ac.uk

Citation:

Mengoli, G., Agustí-Panareda, A., Boussetta, S., Harrison, S. P., Trotta, C., & Prentice, I. C. (2022). Ecosystem photosynthesis in land-surface models: A first-principles approach incorporating acclimation. *Journal of Advances in Modeling Earth Systems*, *14*, e2021MS002767. https://doi.org/10.1029/2021MS002767

Received 17 AUG 2021
Accepted 1 DEC 2021

Author Contributions:

Conceptualization: Giulia Mengoli, Anna Agustí-Panareda, Souhail Boussetta, Sandy P. Harrison, I. Colin Prentice
Data curation: Giulia Mengoli, Carlo Trotta
Formal analysis: Giulia Mengoli
Funding acquisition: I. Colin Prentice
Investigation: Giulia Mengoli

© 2021 The Authors. Journal of Advances in Modeling Earth Systems published by Wiley Periodicals LLC on behalf of American Geophysical Union. This is an open access article under the terms of the Creative Commons Attribution License, which permits use, distribution and reproduction in any medium, provided the original work is properly cited.

Abstract Vegetation regulates land-atmosphere, water, and energy exchanges and is an essential component of land-surface models (LSMs). However, LSMs have been handicapped by assumptions that equate acclimated photosynthetic responses to the environment with the fast responses observable in the laboratory. The effects of acclimation can be taken into account by including PFT-specific values of photosynthetic parameters, but at the cost of increasing parameter requirements. Here, we develop an alternative approach for including acclimation in LSMs by adopting the P model, an existing light-use efficiency model for gross primary production (GPP) that implicitly predicts the acclimation of photosynthetic parameters on a weekly to monthly timescale via optimality principles. We demonstrate that it is possible to explicitly separate the fast and slow photosynthetic responses to environmental conditions, allowing the simulation of GPP at the sub-daily timesteps required for coupling in an LSM. The resulting model reproduces the diurnal cycles of GPP recorded by eddy-covariance flux towers in a temperate grassland and boreal, temperate and tropical forests. The best performance is achieved when biochemical capacities are adjusted to match recent midday conditions. Comparison between this model and the operational LSM in the European Centre for Medium-range Weather Forecasts climate model shows that the new model has better predictive power in most of the sites and years analyzed, particularly in summer and autumn. Our analyses suggest a simple and parameter-sparse method to include both instantaneous and acclimated responses within an LSM framework, with potential applications in weather, climate, and carbon-cycle modeling.

Plain Language Summary Vegetation regulates the exchanges of energy, water, and carbon dioxide between the land and the atmosphere. Numerical climate models represent these processes, focusing mainly on their rapid variations in response to changes in the environment (including temperature and light) on timescales of seconds to hours. However, plants also adjust their physiology to environmental changes over longer periods within the season. Here, we have adapted a simple model that formulates plant behavior in terms of optimal trade-offs between different processes, so it simulates processes on both timescales. This model correctly reproduces the daily cycle of carbon dioxide uptake by plants, as recorded in different kinds of vegetation. We show that plants optimize their behavior for midday conditions, when the light is greatest, and adjust to longer-term environmental variations on a timescale of a week to a month. The model conveniently avoids the need to give specific, fixed values to physiological variables (such as photosynthetic capacity) for different types of plants. The optimality assumptions mean that the model gives equally good results in tropical, temperate, and boreal forests, and in grasslands, using the same equations, and a very small number of input variables.

1. Introduction

Vegetation plays a key role in the Earth system, regulating carbon, water, and energy exchanges between vegetation and atmosphere. Transpiration, photosynthesis, and respiration are the main processes that govern these exchanges and link vegetation to the climate (Bonan, 2008; Bonan et al., 1992, 2003). Evapotranspiration (ET, with accompanying latent-heat release) and photosynthesis are tightly linked. Transpiration is the dominant component of ET, hence plants are the main conduit of water from the soil to the atmosphere. Plants control both transpiration and the flux of carbon dioxide (CO_2) into leaves by regulating the opening or closing of stomata.

19422466, 2022, 1, Downloaded from https://agupubs.onlinelibrary.wiley.com/doi/10.1029/2021MS002767 by Test, Wiley Online Library on [19/07/2024]. See the Terms and Conditions (https://onlinelibrary.wiley.com/terms-and-conditions) on Wiley Online Library for rules of use; OA articles are governed by the applicable Creative Commons License

Methodology: Giulia Mengoli, I. Colin Prentice
Resources: Anna Agustí-Panareda, Souhail Boussetta
Software: Giulia Mengoli, Carlo Trotta
Supervision: I. Colin Prentice
Validation: Giulia Mengoli
Visualization: Giulia Mengoli
Writing – original draft: Giulia Mengoli, Sandy P. Harrison, I. Colin Prentice
Writing – review & editing: Giulia Mengoli, Anna Agustí-Panareda, Souhail Boussetta, Sandy P. Harrison, Carlo Trotta, I. Colin Prentice

Through photosynthesis plants convert solar radiation into growth, storing carbon that otherwise would remain in the atmosphere as a climate-modifying greenhouse gas. CO_2 is removed from the atmosphere by photosynthesis, but released again by autotrophic (plant) and heterotrophic (soil microbial) respiration (Ciais et al., 2013). Contemporary land surface models (LSMs) represent all these interactions. Nevertheless, LSMs make inconsistent future projections of changes in the carbon and water cycles under the same future scenarios (Ciais et al., 2013; Prentice et al., 2015). They do not predict global primary production and its interannual variability correctly (Anav et al., 2015), and differ greatly, for example, in the responses of photosynthesis to temperature and CO_2 (Anav et al., 2013). These issues suggest that the treatment of plant responses to environmental changes in LSMs needs improvement.

Plants respond to environmental changes on multiple timescales. At the ecosystem level, plants adapt to environmental changes on timescales of decades to centuries through competition and migration, such that species replacement maintains ecosystems that are optimally adjusted to the environment at a given location. However, at leaf level, plants respond to environmental changes on shorter timescales. Short-term (fast) responses occur almost instantaneously (seconds to hours). These are the plant responses to environmental stimuli before any type of physiological, structural, or biochemical adjustment, such as synthesizing new enzymes (e.g., Rubisco), occurs. Longer-term responses–known as acclimation—occur over timescales of days to weeks (Mäkelä et al., 2019) or longer (Prentice & Cowling, 2013; Smith & Dukes, 2013). These are physiological and structural adjustments that ensure that plants optimize their behavior to match environmental conditions on weekly to monthly timescales. Plant acclimation is manifested as alterations in the short-term response functions of physiological processes (Smith & Dukes, 2013), such as setting a "basal" amount of enzyme or increasing the optimal temperature for photosynthesis, as a result of past environmental conditions. Key photosynthetic traits, such as the maximum rate of carboxylation (V_{cmax}) or the maximum rate of electron transport (J_{max}) vary systematically with growth conditions, both in space and in time (Rogers et al., 2017; Togashi et al., 2018) due to acclimation.

Many current LSMs describe only the instantaneous responses of photosynthesis to environmental conditions. Originally LSMs used prescribed, plant functional type (PFT)-dependent values for photosynthetic traits. Modern versions of these models recognize the spatial and temporal variability of these traits within PFTs as a function of environmental conditions and thus include dynamic responses of photosynthetic (e.g., ORCHIDEE and JSBACH; see Figure 3 and Table 3 in Smith & Dukes, 2013) and (autotrophic) respiratory processes to temperature (e.g., JULES and CLM4.5). The approach used to account for plant acclimation remains a model parametrization, and therefore the differences between PFTs are maintained (Atkin et al., 2008; Kattge & Knorr, 2007; Lawrence et al., 2019; Lombardozzi et al., 2015). Furthermore, the inclusion of acclimation generally involves additional parameters, with a consequent increase in model complexity (Fisher & Koven, 2020). Attempts have been made to include plant acclimation to light in soil-vegetation-atmosphere (SVAT) models (e.g., Meir et al., 2002) and terrestrial biosphere (TBM) models (e.g., Luo & Keenan, 2020) but most current LSMs do not address all aspects of acclimation. Many studies (e.g., Smith et al., 2019; Walker et al., 2017) have stressed the importance of including acclimation in models—using photosynthetic parameters that vary according to the climate—and indicated that this should lead to improved future projections. It has also been suggested that models that do not account for acclimation might overestimate the positive feedback between climate and vegetation in future scenarios (Smith et al., 2017).

Models of leaf behavior based on eco-evolutionary optimality theory (Franklin et al., 2020; Harrison et al., 2021), where eco-evolutionary refers to the fact that plants adjust to environmental conditions on both ecological and evolutionary timescales and implicitly account for acclimation (Smith et al., 2019; Wang et al., 2017, 2020). However, these models have not been applied at the sub-daily timestep required for an LSM. To do this, it is necessary to treat the instantaneous and acclimated responses of photosynthesis separately.

In this study, we apply an existing optimality-based model for gross primary production (GPP), the P model (Stocker et al., 2020; Wang et al., 2017), to evaluate the potential of modeling the two timescales in a parsimonious way. We extend the model to include both the instantaneous and acclimated responses in the simulation of GPP at a sub-daily timestep, by adopting two alternative averaging methods that allow explicit differentiation between the two responses. We test the resulting version of the P model at sub-daily timesteps using GPP derived from eddy covariance flux-tower measurements from boreal, temperate, and tropical forests and also at a temperate grassland site over different seasons and multiple years. We compare the model performance to that of the CHTESSEL LSM (Balsamo et al., 2009; Boussetta, Balsamo, Beljaars, Panareda, et al., 2013) used at the

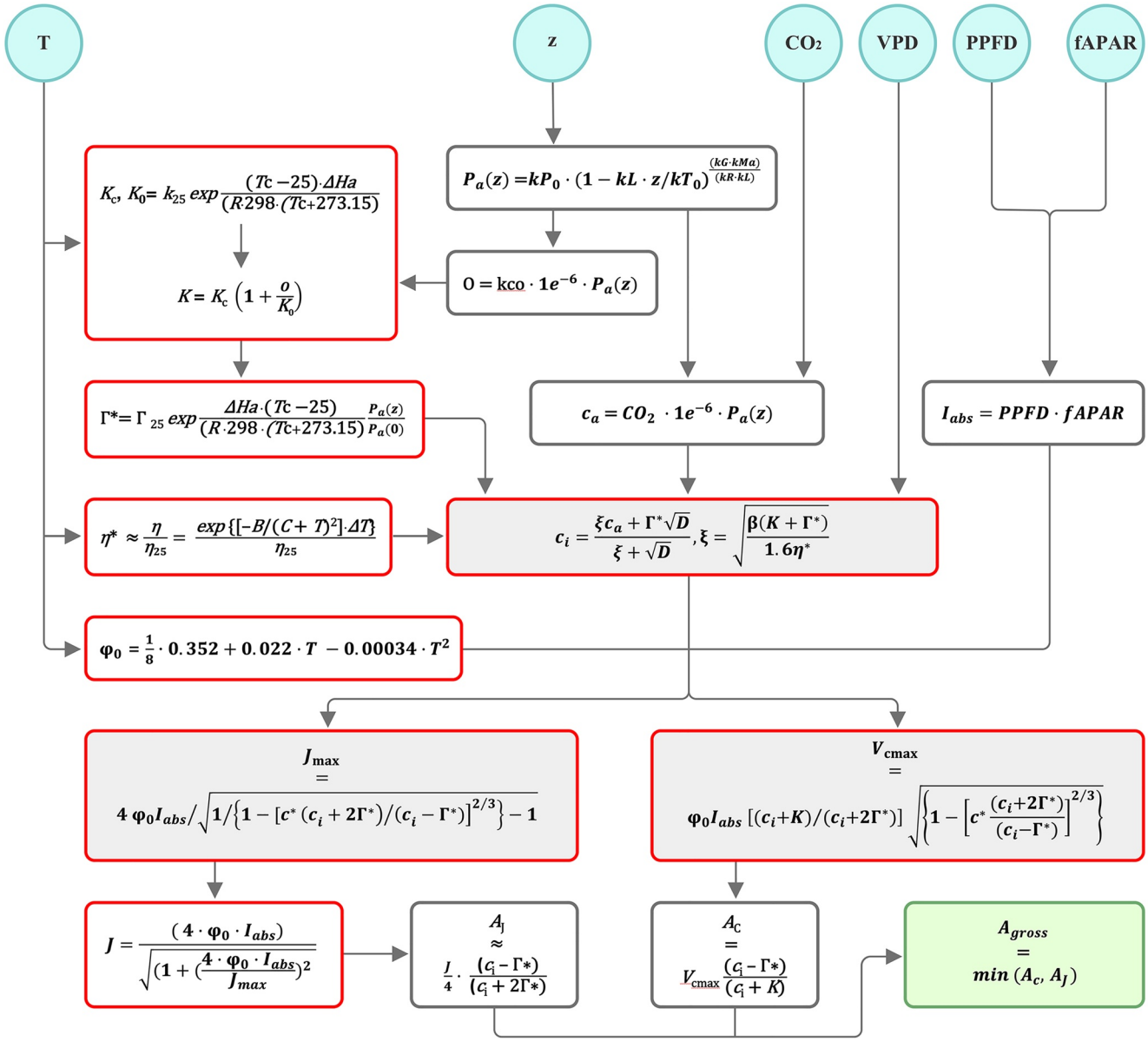

Figure 1. Flowchart of the P model. The model inputs (shown in blue circles) are air temperature (T; °C), site elevation (z; m), ambient carbon dioxide (CO_2; $\mu molCO_2\ mol^{-1}$), vapor pressure deficit (VPD; Pa), photosynthetic photon flux density (PPFD; µmol Photon $m^{-2}\ s^{-1}$) and the fraction of absorbed photosynthetically active radiation (fAPAR; unitless). The red rectangles are the temperature dependent parameters and the green rectangle is the model output. Parameter definitions are given in Table 1. For details of the P model equations see Wang et al. (2017) and Stocker et al. (2020).

European Centre for Medium-Range Weather Forecasts (ECMWF). This extended version of the P model reproduces the diurnal cycle of GPP through the growing seasons of multiple years and is generally more accurate than CHTESSEL, with no need for changing parameters between biomes. Our work thus provides a proof-of-concept for including acclimated responses in an LSM framework.

2. Materials and Methods

2.1. The P Model

The P model (Wang et al., 2017) is an optimality-based model of GPP driven by solar radiation, temperature, vapor pressure deficit (VPD), ambient CO_2, and the fraction of absorbed photosynthetically active radiation (fAPAR), which is assumed to be related to leaf area index (LAI) by Beer's law (Stocker et al., 2020; Figure 1).

19422466, 2022, 1, Downloaded from https://agupubs.onlinelibrary.wiley.com/doi/10.1029/2021MS002767 by Test, Wiley Online Library on [19/07/2024]. See the Terms and Conditions (https://onlinelibrary.wiley.com/terms-and-conditions) on Wiley Online Library for rules of use; OA articles are governed by the applicable Creative Commons License

19422466, 2022, 1, Downloaded from https://agupubs.onlinelibrary.wiley.com/doi/10.1029/2021MS002767 by Test, Wiley Online Library on [19/07/2024]. See the Terms and Conditions (https://onlinelibrary.wiley.com/terms-and-conditions) on Wiley Online Library for rules of use; OA articles are governed by the applicable Creative Commons License

Table 1
Definitions of Photosynthetic Parameters, Rates, and Constants Used in the P Model

Symbol	Description	Unit or value	Reference
V_{cmax}	Maximum rate of carboxylation (or maximum rate of Rubisco activity)	μmol CO_2 m^{-2} s^{-1}	Wang et al., 2017
ΔH_a	Activation energy for V_{cmax}	65 330 [J mol^{-1}]	Bernacchi et al., 2001
J_{max}	Maximum rate of electron transport	μmol electrons m^{-2} s^{-1}	Wang et al., 2017
ΔH_{aj}	Activation energy for J_{max}	43 990 [J mol^{-1}]	Bernacchi et al., 2003
R	Universal gas constant	8.314 [J mol^{-1} K^{-1}]	——
$\chi = c_i{:}c_a$	Ratio of leaf-internal to ambient partial pressures of CO_2	Unitless	Prentice et al., 2014; Wang et al., 2017
c_i	Leaf-internal CO_2 partial pressure	Pa	Wang et al., 2017
c_a	Ambient CO_2 partial pressure	Pa	
ξ	Sensitivity of χ to vapor pressure deficit (VPD or D)	$Pa^{1/2}$	Wang et al., 2017
g_s	Stomatal conductance to CO_2	μmol CO_2 m^{-2} s^{-1}	Medlyn et al., 2011; Prentice et al., 2014
$\varphi_0(T)$	Temperature dependence function of quantum efficiency	mol mol^{-1}	Bernacchi et al., 2003
β	The ratio of cost factors for carboxylation and transpiration capacities at 25°C	146 (unitless)	Stocker et al., 2020
c^*	The cost factor for electron-transport capacity	0.41 (unitless)	Wang et al., 2017
K_C	Michaelis-Menten constant for carboxylation	Pa	Farquhar et al., 1980; Bernacchi et al., 2001
K_{C25}	Michaelis-Menten constant for carboxylation at 25°C	39.97 [Pa]	Bernacchi et al., 2001
ΔH_{KC}	Activation energy for K_C	79 430 [J mol^{-1}]	Bernacchi et al., 2001
K_O	Michaelis-Menten constant for oxygenation	Pa	Farquhar et al., 1980; Bernacchi et al., 2001
Ko_{25}	Michaelis-Menten constant for oxygenation at 25°C	27 480 [Pa]	Bernacchi et al., 2001
ΔH_{Ko}	Activation energy for Ko	36 380 [J mol^{-1}]	Bernacchi et al., 2001
K	The effective Michaelis-Menten coefficient for Rubisco kinetics	Pa	Farquhar et al., 1980
Γ*	Photorespiratory compensation point	Pa	Farquhar et al., 1980; Bernacchi et al., 2001
Γ^*_{25}	Photorespiratory compensation point at 25°C	4.332 [Pa]	Bernacchi et al., 2001
ΔH_{Γ^*}	Activation energy for Γ*	37 830 [J mol^{-1}]	Bernacchi et al., 2001
η^*	Temperature dependence of the viscosity of the water, relative to its value at 25°C	unitless	Huber at al. 2009
$P_a(z)$	Atmospheric pressure at given elevation (z)	Pa	Berberan-Santos et al., 1997
J	Rate of electron transport	μmol electrons m^{-2} s^{-1}	Smith, 1937
A_C	Rubisco-limited assimilation rate	μmol CO_2 m^{-2} s^{-1}	Farquhar et al., 1980
A_J	Electron-transport limited assimilation rate	μmol CO_2 m^{-2} s^{-1}	Farquhar et al., 1980
A	Assimilation rate	μmol CO_2 m^{-2} s^{-1}	Farquhar et al., 1980

Although most applications of the P model have used satellite-derived fAPAR data as inputs (Stocker et al., 2020; Wang et al., 2017), the model has also been run by estimating LAI from predicted GPP (Qiao et al., 2020) thus making it possible to project future conditions. In this study, we use satellite-derived fAPAR to develop the approach to separating the instantaneous and acclimated timescales, but then use observed LAI data for the comparison with CHTESSEL. The P model is based on the Farquhar et al. (1980) biochemical model of photosynthesis (FvCB), but incorporates additional eco-evolutionary optimality hypotheses, which express the acclimation of plant photosynthetic capacities and stomatal behavior to environmental changes: the coordination hypothesis (Maire et al., 2012) and the least-cost hypothesis (Prentice et al., 2014). The coordination hypothesis states that plants tend to optimize their performance by adjusting their photosynthetic capacities (V_{cmax} and J_{max}, Table 1) to use all of the available light. This leads to the conclusion that V_{cmax} and J_{max} should be continually adjusted to environmental variations according to general rules that do not depend on PFTs. The least-cost hypothesis states

19422466, 2022, 1, Downloaded from https://agupubs.onlinelibrary.wiley.com/doi/10.1029/2021MS002767 by Test, Wiley Online Library on [19/07/2024]. See the Terms and Conditions (https://onlinelibrary.wiley.com/terms-and-conditions) on Wiley Online Library for rules of use; OA articles are governed by the applicable Creative Commons License

that plants minimize the sum of carbon and water costs—in terms of the maintenance costs for transpiration and carboxylation capacities. This hypothesis leads to an optimal ratio of the leaf-internal to ambient CO_2 partial pressure (c_i:c_a, Table 1) applicable to all C_3 plants.

The P model implicitly represents plant adaptation and acclimation, via photosynthetic capacity and stomatal behavior, over a timescale of days to weeks. It reproduces observed variation in V_{cmax}, J_{max}, and stomatal conductance for CO_2 (g_s, Table 1) along environmental gradients (Bloomfield et al., 2019; Dong et al., 2020; Smith et al., 2019; Wang et al., 2017, 2020). It also includes the measured effect of low temperatures on the intrinsic quantum efficiency of photosynthesis ($\varphi_0(T)$: Table 1) (Rogers et al., 2017, 2019; Singsaas et al., 2001). The parameters in the P model are either approximately constant and known from independent physiological studies, or estimated from analyses of independent data (c^* and β: see Table 1). The P model performs as well as more parameter-rich models (e.g., Zhang et al., 2019) at weekly to monthly time steps (Stocker et al., 2020), that is, at the timescale of acclimation of key quantities such as V_{cmax} and J_{max}.

2.2. Timescales of Acclimation

To implement the P model at a sub-daily timestep requires an explicit distinction between the fast (instantaneous) response of photosynthetic rates (*Ac*, A_j: Figure 1) and the slower acclimated response of photosynthetic traits (V_{cmax}, J_{max}, and ξ: Figure 1). To account for the acclimation of photosynthetic traits we first use a method that involves computing a running mean of model inputs over a defined antecedent period. With this method, we tested three approaches to find the optimal timescale for acclimation: the "daily" approach computes a running mean of average daytime conditions; the "3 hr" approach considers an average of three values from the middle of each day; the "noon" approach considers only conditions around midday. The inputs are used to obtain the optimal values of V_{cmax} and J_{max} (Equations 1 and 2). These represent the slow (acclimated) responses of the photosynthetic traits (Wang et al., 2017):

$$V_{cmax}[\text{opt}] = \varphi_0 I_{abs} \frac{(c_i + K)}{(c_i + 2\Gamma^*)} \sqrt{1 - \left[c^* \frac{(c_i + 2\Gamma^*)}{(c_i - \Gamma^*)}\right]^{\frac{2}{3}}} \quad (1)$$

$$J_{max}[\text{opt}] = \frac{4\ \varphi_0 I_{abs}}{\sqrt{\frac{1}{1 - \left[\frac{c^*(c_i + 2\Gamma^*)}{(c_i - \Gamma^*)}\right]^{\frac{2}{3}}} - 1}} \quad (2)$$

where c_i is the leaf-internal CO_2 partial pressure (Pa), Γ^* is the photorespiratory compensation point (Pa), K is the effective Michaelis-Menten coefficient (Pa), φ_0 is the intrinsic quantum efficiency of photosynthesis (mol mol^{-1}), following the temperature dependence function φ_0 (T) reported in Bernacchi et al. (2003), I_{abs} is the absorbed light, which is a product of the incoming photosynthetic photon flux density (PPFD, μmol photon $m^{-2}s^{-1}$) and fAPAR. $c^* = 0.41$ is a cost factor for electron transport capacity.

A standard function for the temperature response of V_{cmax} and J_{max}, the Arrhenius equation (Equation 3), is then used to adjust both photosynthetic traits from the average (optimal) temperature to the actual temperature (Equations 3a and 3b). This adjustment for each half-hourly timestep represents the instantaneous response in the model.

$$\text{param}\ (T_1) = \text{param}\ (T_0)\ \exp\left[\left(\frac{\Delta H_a}{R}\right)\left(\frac{1}{T_0} - \frac{1}{T_1}\right)\right] \quad (3)$$

$$V_{cmax}\text{adjusted} = V_{cmax}[\text{opt}]\ \exp\left[\left(\frac{\Delta H_a}{R}\right)\left(\frac{1}{T_0} - \frac{1}{T_1}\right)\right] \quad (3a)$$

$$J_{max}\text{adjusted} = J_{max}[\text{opt}]\ \exp\left[\left(\frac{\Delta H_{aj}}{R}\right)\left(\frac{1}{T_0} - \frac{1}{T_1}\right)\right] \quad (3b)$$

19422466, 2022, 1, Downloaded from https://agupubs.onlinelibrary.wiley.com/doi/10.1029/2021MS002767 by Test, Wiley Online Library on [19/07/2024]. See the Terms and Conditions (https://onlinelibrary.wiley.com/terms-and-conditions) on Wiley Online Library for rules of use; OA articles are governed by the applicable Creative Commons License

where T_0 is the average temperature computed by a 15-day running mean (K) and T_1 is the actual half-hourly temperature (K), R is the universal gas constant, and ΔH_a (ΔH_{aj}) is the activation energy (J mol^{-1}). The parameter values used in the Arrhenius equation are those measured by Bernacchi et al. (2001, 2003) and listed in Table 1.

Using the same logic for the stomatal conductance, we include a dynamic optimization of stomatal conductance operating on the c_i:c_a ratio (χ, Equation 4) to obtain acclimated and optimal values of ξ, a parameter that determines the sensitivity of χ to VPD (Prentice et al., 2014). The acclimated response of ξ to environmental conditions (see e.g., Lin et al., 2015; Marchin et al., 2016) — is included in the c_i formula (Equation 5), which is then immediately updated at every half-hourly timestep with the actual VPD to include the fast response of stomata to VPD:

$$\chi = \frac{\Gamma^*}{c_a} + \frac{(1 - \Gamma^*/c_a)\xi}{\xi + \sqrt{D}} \tag{4}$$

$$c_i = \frac{\xi c_a + \Gamma^* \sqrt{D}}{\xi + \sqrt{D}}, \quad \xi = \sqrt{\frac{\beta(K + \Gamma^*)}{1.6\eta^*}} \tag{5}$$

where c_i is the leaf-internal and c_a is the ambient CO_2 partial pressure (Pa), D is the vapor pressure deficit (Pa), β = 146 is the ratio of the cost factors for carboxylation and transpiration capacities (at 25°C) (Stocker et al., 2020), and η^* is the viscosity of water relative to its value at 25°C.

The acclimated parameters (V_{cmax}, J_{max}, χ and thus c_i), adjusted to the actual conditions (Equations 3a, 3b, and 5) and the instantaneous parameters –c_i, K and Γ*- are used to compute the photosynthetic assimilation rates (A_c and A_j: Table 1). These are the two limiting rates for carbon assimilation; their minimum value gives the GPP.

2.3. Incorporating Acclimation in a Land-Surface Modeling Framework

Storing daily data to compute a running-mean would be computationally costly in an LSM context. We therefore tested whether the longer-term acclimation timescales could be mimicked based on a technique used to incorporate memory in other aspects of climate modeling, the exponential weighted moving average method. This method, here called the weighted mean approach, is used in forecasting systems that deal with inaccurate prediction caused by the insufficiency of historical observations and allows for a self-starting forecasting process without having to store past data (Yu et al., 2020). The method is used in a variety of applications in forecasting, from estimating soil moisture from precipitation (Campos de Oliveira et al., 2017) to vegetation acclimation processes (e.g., Vanderwel et al., 2015).

This weighted mean approach is an alternative way to manage the fast and slow responses of plants to environmental changes. It uses the exponential moving average (EMA) equation (see Text S1, Equation 7 in Supporting Information S1) – which computes a mean in which the contribution of antecedent days decays exponentially with distance from the present–to obtain the acclimated parameters and the reciprocal and canonical forms of the Arrhenius equations (see Text S1, Equations 6 and 8 in Supporting Information S1) to obtain the instantaneous values of V_{cmax} and J_{max}. Thus, the weighted mean approach differs from the running mean approach in that it is applied to the photosynthetic variables V_{cmax}, $J_{max,}$ and c_i directly rather than to model inputs. We use these biochemical quantities at standard temperature (25°C), V_{cmax25} and J_{max25} to emulate what happens in nature. V_{cmax25} reflects the quantity of active Rubisco in the canopy. Plants adjust the amount of Rubisco (V_{cmax25}) slowly; it cannot, for example, change during the night when photosynthesis does not occur. The "basal" amount of Rubisco is related to past conditions, the actual V_{cmax} at any one timestep is adjusted from the basal rate by enzyme kinetics.

The weighted mean approach is applied as follows. First, optimal V_{cmax} and J_{max} (Equations 1 and 2) are computed based on conditions at noon; then, V_{cmax25} and J_{max25} are obtained using the reciprocal formula of the Arrhenius equation (h^{-1}; see, Text S1, Equation 3a*** in Supporting Information S1) (see Text S1, Equation 6 in Supporting Information S1) and used in the EMA equation. Computing the EMA equation, the acclimated responses of V_{cmax25} and J_{max25} (for the current day) are obtained and then, using the canonical form of the Arrhenius equation (see, Text S1, Equation 8 in Supporting Information S1), the instantaneous responses of both photosynthetic traits are computed at each half-hourly timestep. Like V_{cmax25} and J_{max25}, ξ should vary slowly; however, ξ has no "fast" reaction to temperature, so the Arrhenius function is not needed. After having obtained ξ for the current day, c_i is

19422466, 2022, 1, Downloaded from https://agupubs.onlinelibrary.wiley.com/doi/10.1029/2021MS002767 by Test, Wiley Online Library on [19/07/2024]. See the Terms and Conditions (https://onlinelibrary.wiley.com/terms-and-conditions) on Wiley Online Library for rules of use; OA articles are governed by the applicable Creative Commons License

adjusted with the fast variation in VPD for each half-hourly timestep. Finally, these acclimated parameters—also adjusted to match the actual environmental conditions—are used to compute both photosynthetic rates (Ac, A_J) and thus GPP at a sub-daily timestep.

To initialize the model simulations, we assume that on the very first day available in the data set, the acclimated responses of V_{cmax25} or J_{max25} ($V_{25,}$ Equation 7 in Supporting Information S1) are given by $V_{25,\mathrm{opt}}$ only. The weight of $V_{25,\mathrm{opt}}$ decreases exponentially as time progresses (see Text S1, Equation 9 in in Supporting Information S1). So, it is necessary to spin-up the model for about 2 months before evaluation of model performance. Then, we apply Equation 7 in Supporting Information S1 as discussed previously.

The EMA equation includes a parameter (α), the constant smoothing factor. According to Equation 9, Text S1 in Supporting Information S1, α = 0.067 corresponds to about 15 days of memory. We therefore set $\alpha = 0.067$ for consistency with the running mean method. We also tested a range of alternative values of α: 0.33, 0.143, 0.1, 0.067, 0.033, 0.022, and 0.0167, corresponding to 3, 7, 10, 15, 30, 45, and 60 days, respectively.

2.4. The CHTESSEL Model

We compare predictions from our extended P model to results from the ECMWF operational LSM, CHTESSEL (Balsamo et al., 2009; Boussetta, Balsamo, Beljaars, Panareda, et al., 2013). This is the new version of the Hydrology-Tiled ECMWF scheme for Surface Exchange over Land (H-TESSEL) (Balsamo et al., 2009; Viterbo et al., 1999), where the interface between the surface and the atmosphere is represented by grid-boxes, which are tiled according to surface characteristics and grid-box fluxes are calculated for each tile (mosaic approach). It thus includes many PFT-specific fixed parameters. CHTESSEL includes a photosynthesis-stomatal conductance sub-model (A-gs, Jacobs, 1994; Jacobs et al.,1996) in its CO_2 exchange module, but does not include any explicit representation of acclimation. CHTESSEL is part of the ECMWF operational model, the Integrated Forecast System (IFS), which is an atmospheric model and data assimilation system. When the LSM is fully coupled to the atmospheric model in IFS, then vegetation and CO_2 fluxes are modeled online within IFS. However, here we test the model in offline mode driven by the same environmental variables (solar radiation, temperature, atmospheric CO_2, and atmospheric humidity deficit) measured at eddy-covariance flux tower sites.

2.5. Data and Evaluation

We initially compared P model predictions with sub-daily observations from five sites from the FLUXNET2015 data set (Pastorello et al., 2020) using the most recent common year (2014) for all five sites. We chose sites that represent a range of climate and vegetation types (Table 2): boreal forest (FI-Hyy), temperate deciduous broadleaf (US-UMB) and mixed (BE-Vie) forests, tropical forest (GF-Guy), and temperate grassland (CH-Cha). The FLUXNET data set provide meteorological variables (PPFD_IN, VPD_F, TA_F, and CO2_F_MDS) on a half-hourly timestep at each site, as well as observed GPP. We used GPP based on the daytime partitioning method (GPP_DT_CUT_REF) (Lasslop et al., 2010; Pastorello et al., 2020). Since the FLUXNET2015 data set does not provide fAPAR, we obtained this from the MCD15A3H Collection 6 data set (Myneni et al., 2015). The MODIS FPAR product has a spatial resolution of 500 m and a temporal resolution of four days. We used the version of these data from Stocker et al. (2020) that has been filtered to remove data points where clouds were present and linearly interpolated from 4 days to daily. We used linear interpolation to derive fAPAR on the same sub-daily temporal resolution as the meteorological forcing.

We then performed more extensive evaluations based (a) on an additional five sites from the FLUXNET2015 data set and (b) examining additional years at all 10 sites. The additional sites were chosen to represent the same five biomes used in the initial analysis (Table 2). We compared observed and simulated GPP over the growing season, where the growing season at each site was determined using the threshold approach defined by Lasslop et al. (2012). This approach defines the start and end of the growing season as the days that correspond to GPP values of >20% of the 0.05 and 0.95 quantile range. We also selected individual weeks corresponding to the early growing season (spring), the peak growing season (summer), and the late growing season (autumn) to examine whether model performance varied seasonally.

The FLUXNET2015 data set provides information about the quality of data, through the quality-flag variables (see supplementary Table SM1 in Pastorello et al., 2020). We removed data points where the quality control (QC)

19422466, 2022, 1, Downloaded from https://agupubs.onlinelibrary.wiley.com/doi/10.1029/2021MS002767 by Test, Wiley Online Library on [19/07/2024]. See the Terms and Conditions (https://onlinelibrary.wiley.com/terms-and-conditions) on Wiley Online Library for rules of use; OA articles are governed by the applicable Creative Commons License

Table 2
Summary of the Characteristics of the FLUXNET2015 Sites Used for Model Evaluation

Site name	Site ID	Latitude (°)	Longitude (°)	Elevation (m)	MAT (°C)	MAP (mm)	IGBP vegetation type
Hyytiälä	FI-Hyy	61.84741	24.29477	181	3.8	709	Evergreen needleleaf forest
Vielsalm	BE-Vie	50.30493	5.99812	493	7.8	1062	Mixed forest
University of Michigan Biological Station	US-UMB	45.5598	−84.7138	234	5.8	803	Deciduous broadleaf forest
French Guiana	GF-Guy	5.27877	−52.92486	48	25.7	3041	Evergreen broadleaf forest
Chamau	CH-Cha	47.21022	8.41044	393	9.5	1136	Grassland
Fyodorovskoye	RU-Fyo	56.4615	32.9221	265	3.9	711	Evergreen needleleaf forest
Sylvania Wilderness Area	US-Syv	46.2420	−89.3477	540	3.8	826	Mixed forest
Morgan Monroe State Forest	US-MMS	39.3232	−86.4131	275	10.9	1032	Deciduous broadleaf forest
Santarem-Km83-Logged Forest	BR-Sa3	−3.0180	−54.9714	100	26.1	2044	Evergreen broadleaf forest
Grillenburg	DE-Gri	50.9500	13.5126	385	7.8	901	Grassland

Note. MAT: mean annual temperature (°C); MAP: mean annual precipitation (mm).

is flagged as medium or poor prior to comparison with model outputs. We computed the percentage of "good" observations for each year analyzed. Times when there are no meteorological or GPP observations are necessarily ignored in the comparisons. There is no information that can be used to assess the quality of the fAPAR data and LAI data.

Model goodness-of-fit was measured using R^2, root-mean square error (RMSE), relative root-mean square error (nRMSE, which is the RMSE normalized by the standard deviation of the observations), and the bias error (BE). These metrics have been computed using the "hydroGOF" R package. The median RMSE, nRMSE, $R^{2,}$ and BE, were obtained by computing an RMSE, nRMSE, $R^{2,}$ and BE for each half hour of every week during the growing season at each site. We estimated the number of weeks when model performance was reasonable by examining the RMSE distribution to determine a threshold to exclude outliers, which might be associated with data uncertainties. The weeks used to illustrate the comparisons with observations were chosen because they have the maximum number of reliable observations, although complete information is given in the summary tables (Tables S1 and S2 in Supporting Information S2).

Table 3
Summary of Model Performance Statistics (RMSE Is the Root Mean Square Error, R^2 Is the Coefficient of Determination, and BE Is the Bias or Systematic Error) to Compare the Use of Three Approaches (i.e., Daily, 3 Hours, and Noon) Over the Growing Season at Five Flux Tower Sites in 2014

Site ID	Year	Approaches	Median RMSE	Median R^2	Median BE
BE-Vie	2014	Daily	2.69	0.91	−0.92
BE-Vie	2014	3 hr	2.07	0.93	−0.19
BE-Vie	2014	Noon	2.28	0.94	0.01
FI-Hyy	2014	Daily	2.74	0.86	−0.51
FI-Hyy	2014	3 hr	2.43	0.90	0.86
FI-Hyy	2014	Noon	2.53	0.91	0.99
GF-Guy	2014	Daily	3.35	0.95	−0.80
GF-Guy	2014	3 hr	2.94	0.97	0.49
GF-Guy	2014	Noon	3.67	0.98	2.04
US-UMB	2014	Daily	3.18	0.84	−0.21
US-UMB	2014	3 hr	3.66	0.88	1.84
US-UMB	2014	Noon	3.54	0.88	1.98
CH-Cha	2014	Daily	5.28	0.83	−1.79
CH-Cha	2014	3 hr	4.53	0.87	0.07
CH-Cha	2014	Noon	3.89	0.88	1.07

We evaluated and compared the performance of the newly developed version of the P model and CHTESSEL in different seasons and over different years at all of the sites. For this comparison we forced both models with the same meteorological inputs and LAI data. The LAI time series were derived from MODIS LAI collection 5 (Boussetta, Balsamo, Beljaars, Kral, & Jarlan, 2013; Myneni et al., 2002). Both models were run in stand-alone mode (i.e., OSM-Ags for CHTESSEL) and tested against the same GPP recorded by eddy-covariance flux towers.

3. Results

We tested the optimal timescale for acclimation to light availability by comparing simulations using average daily inputs, 3-hourly average inputs centered on noon and midday conditions. The use of average daily inputs leads to an underestimation of the observed GPP at all of the test sites, which is substantial (BE: −1.79) at CH-Cha (Table 3). However, model predictions

19422466, 2022, 1, Downloaded from https://agupubs.onlinelibrary.wiley.com/doi/10.1029/2021MS002767 by Test, Wiley Online Library on [19/07/2024]. See the Terms and Conditions (https://onlinelibrary.wiley.com/terms-and-conditions) on Wiley Online Library for rules of use; OA articles are governed by the applicable Creative Commons License

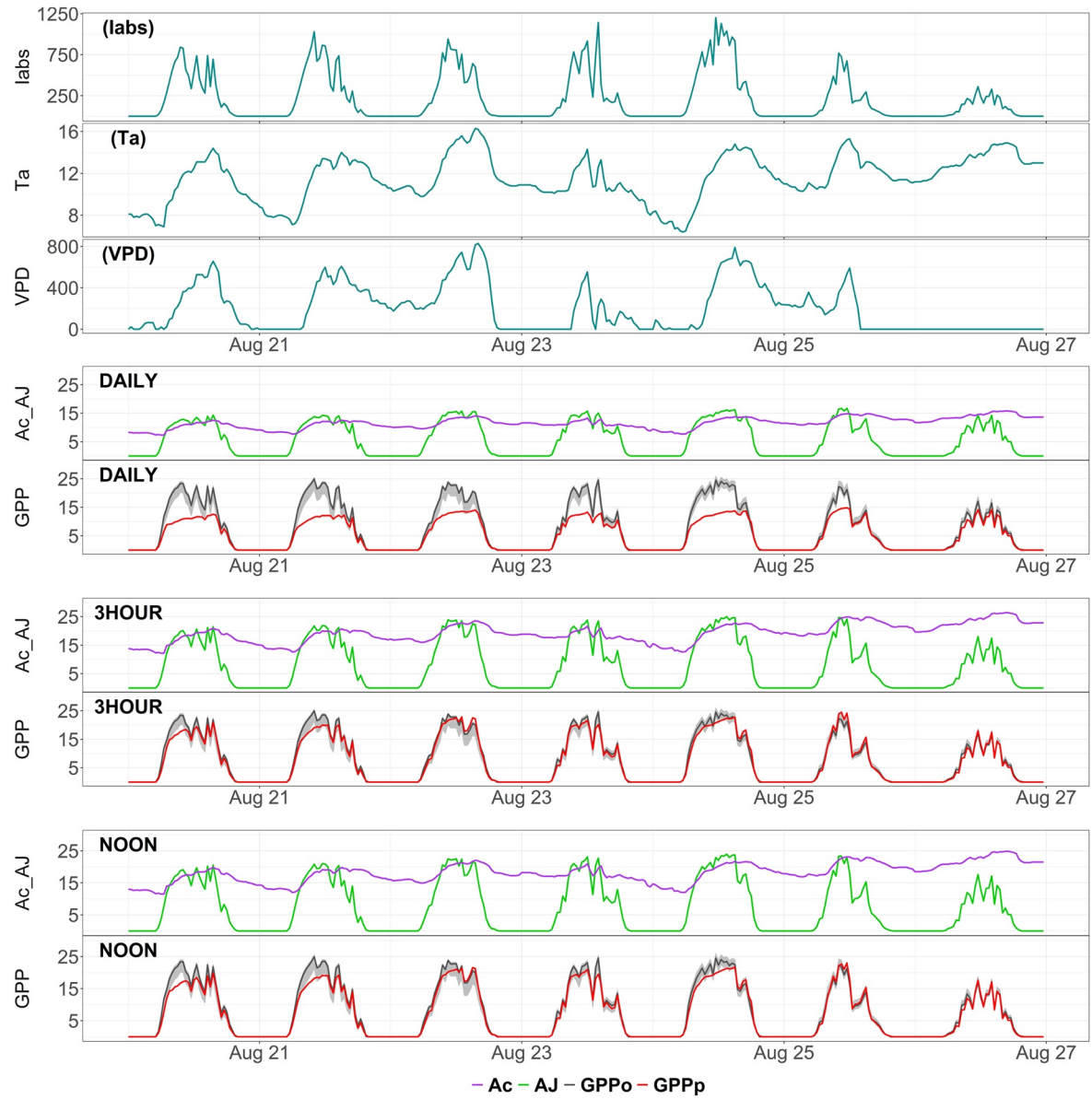

Figure 2. Sub-daily trends in model inputs (absorbed light: Iabs; temperature: Ta; and vapor pressure deficit: VPD) during one week in August 2014 at the Vielsalm (BE-Vie) site and the simulated Rubisco-limited assimilation rate (A_C; μmol CO_2 m^{-2} s^{-1}), electron-transport limited assimilation rate (A_J; μmol CO_2 m^{-2} s^{-1}), and gross primary production (GPP) using the running mean approach with inputs for average daytime conditions (DAILY), averaged over three hours from the middle of the day (3HOUR) and around midday (NOON). The model inputs—Iabs, Ta, and VPD—are in units of μmol Photon m^{-2} s^{-1}, °C and Pa, respectively. Simulated GPP (GPPp) is shown in red and the GPP derived from eddy covariance flux-tower measurements (GPPo) is shown in gray, both expressed in μmol CO_2 m^{-2} s^{-1}. The gray shaded areas represent the uncertainty in GPPo calculated by the daytime partitioning method in the FLUXNET2015 data set.

of GPP using 3-hourly or midday inputs are both consistent with the observations. At BE-Vie (Figure 2), for example, model performance during a single week in August 2014 using average daily inputs is poorer (R^2: 0.92) than either the 3-hourly averages (R^2: 0.98) or midday conditions (R^2: 0.98). This is also the case at the other four sites (Figures S1, S2, S3, and S4 in Supporting Information S2) and considering performance over the whole year (Table 3). The three averaging approaches affect the seasonal trends of the key photosynthetic parameters differently, here illustrated using 2014 as an example. Both V_{cmax} and J_{max} show upward trends in spring (Figure S4a in Supporting Information S2) reaching their maximum values in summer (Figure S4b in Supporting Information S2), then downward trends in the later part of the year (Figure S4c in Supporting Information S2). This general behavior is common to the different averaging approaches, but the daily approach leads to lower values than the other approaches. This difference propagates into sub-daily variations of simulated GPP, which depart

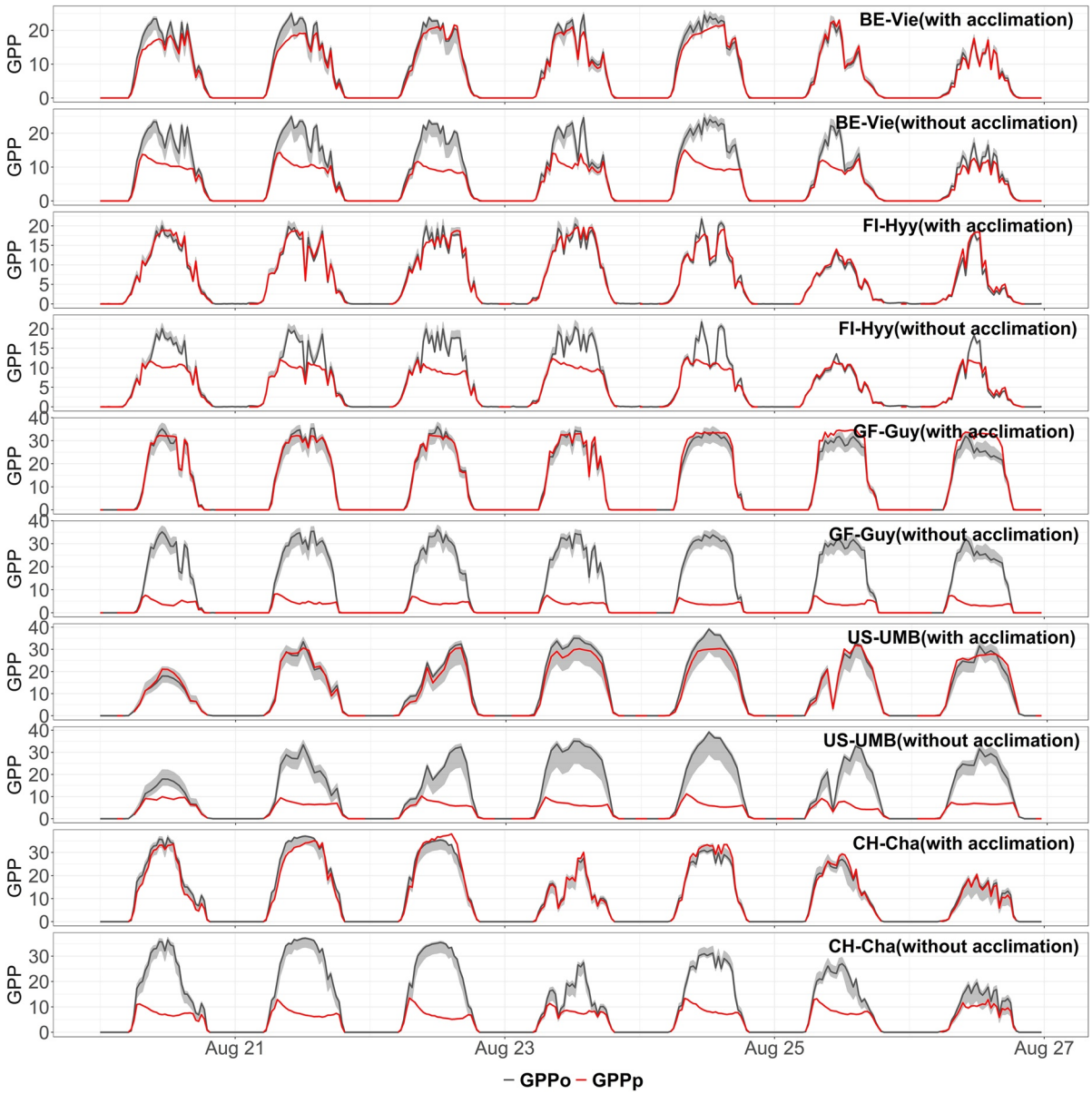

Figure 3. Comparison of simulated gross primary production by the P model "with" and "without acclimation' (GPPp, labeled with site ID and "with acclimation" or "without acclimation") and the GPP derived from eddy covariance flux-tower measurements (GPPo) for a single week in August 2014 at each of the five FLUXNET2015 sites (site IDs are displayed in the top left corner). GPP is expressed in μmol CO_2 m^{-2} s^{-1}. The gray shaded areas represent the uncertainty in GPPo calculated by the daytime partitioning method in the FLUXNET2015 data set.

further from observations if the daily approach is used (Figure S4b in Supporting Information S2). These results support the hypothesis that plants coordinate their biochemical capacities to match the maximum level of light during a day, optimizing to near-midday rather than average daytime conditions.

We designed two tests (A and B) to illustrate the importance of acclimation for P model performance. In Test A, the average value of modeled optimal V_{cmax}, $J_{max,}$ and ξ over the growing season was applied as constants through the year to simulate behavior at the BE-Vie site. In Test B, the constant values of V_{cmax}, $J_{max,}$ and ξ from BE-Vie were applied at the other sites (Figure 3). Applying temporally constant parameter values based on average growing-season conditions led to a greater underestimate of GPP both in summer and autumn (Figures S4e and S4f in Supporting Information S2) and a poorer overall model performance at BE-Vie than when acclimation is allowed to occur (Table S3 in Supporting Information S2). Applying these same values at other sites shows how important

19422466, 2022, 1, Downloaded from https://agupubs.onlinelibrary.wiley.com/doi/10.1029/2021MS002767 by Test, Wiley Online Library on [19/07/2024]. See the Terms and Conditions (https://onlinelibrary.wiley.com/terms-and-conditions) on Wiley Online Library for rules of use; OA articles are governed by the applicable Creative Commons License

Table 4
Summary of Model Performance Statistics at Five Flux Tower Sites in 2014 (RMSE Is the Root Mean Square Error, nRMSE Is the Relative Root Mean Square Error, R^2 Is the Coefficient of Determination, and BE Is the Bias or Systematic Error)

Site ID	No. Weeks	Median RMSE	Median nRMSE	Median R^2	Median BE	% Good Weeks
BE-Vie	52	2.28	39.95	0.94	0.01	86.5%
FI-Hyy	38	2.53	69.65	0.91	0.99	68.4%
GF-Guy	52	3.67	37.25	0.98	2.04	82.7%
US-UMB	37	3.54	110.8	0.88	1.98	83.8%
CH-Cha	52	3.89	53.55	0.88	1.07	80.8%

Note. The number of weeks (No. weeks) is the length of the growing season at each site in 2014. The percentage of good weeks is estimated after excluding those weeks where the RMSE exceeds a threshold value of twice the median RMSE.

it is to account for acclimation to spatial variability in environmental conditions. In summer, while the P model "with acclimation" correctly reproduced diurnal cycles of GPP as recorded by flux tower measurements, the P model "without acclimation" underestimated GPP at all five sites (Figure 3; Figure S4h in Supporting Information S2). In autumn, three of the five sites (i.e., GF-Guy; US-UMB; CH-Cha) showed a large underestimation (Figure S4i in Supporting Information S2), while in spring the P model's tendency to overpredict GPP at some sites was exacerbated (Figure S4g in Supporting Information S2). In comparisons of predicted and observed GPP, all metrics (Table S3 in Supporting Information S2) were consistently better for the P model "with acclimation" than "without acclimation".

Comparison of predicted and observed GPP at all five sites shows that the running-mean model ("with acclimation") accurately mimics the diurnal cycles of GPP (Figure 3). The median R^2 over all weeks (Table 4) ranges from 0.88 (CH-Cha, US-UMB) to 0.98 (GF-Guy). The median RMSE ranges from 3.89 μmol CO_2 m^{-2} s^{-1} (CH-Cha) to 2.28 μmol CO_2 m^{-2} s^{-1} (BE-Vie). The median nRMSE ranges from 69.65% (FI-Hyy) and 37.25% (GF-Guy) to a high value at US-UMB (110.8%) The median BE ranges from 2.04 μmol CO_2 m^{-2} s^{-1} (GF-Guy) to 0.01 μmol CO_2 m^{-2} s^{-1} (BE-Vie). There does not appear to be a relationship between the quality of the model fit and the length of the growing season. The model produces a good fit to observations at most of the sites for at least 80% of the individual weeks in 2014 (Table 4). The poorest performance in terms of number of weeks simulated accurately (68%) is for FI-Hyy and probably reflects uncertainties in the fAPAR inputs for this site. The model overall simulates the sub-daily trends of observed GPP well at these sites for other years (i.e., 2013, 2012, and 2011), showing values of median $R^2 > 0.90$ for four of the five sites, with the lowest value of 0.84 at CH-Cha in 2012 (Table S1 in Supporting Information S2). At annual timescales model simulations are close to the observations, with relatively low values of median BE for most sites (Table S1 in Supporting Information S2).

Comparisons at the additional sites (Table S2 in Supporting Information S2) again confirm that the model performs reasonably well: the median R^2 over all the years and sites ranges from 0.86 to 0.97. Model performance is particularly good at the tropical site BR-Sa3, with a median R^2 of about 0.9 for all four years available in the data set. The median RMSE is high at both US-MMS (6.27 μmol CO_2 m^{-2} s^{-1}) and US-Syv (6.52 μmol CO_2 m^{-2} s^{-1}) in 2013, as is the bias error. The model also overpredicts GPP at these two sites in 2012, resulting in a higher error than the other sites, although the median R^2 is good (0.94: US-MMS; 0.95: US-Syv). Again, high error values are often associated with a lower number of reliable observations. There are only 61% observations available for the US-MMS site in 2013, and 47% for the US-Syv. High errors are also registered at the tropical site (BR-Sa3) in 2000, where there is 46.4% of observations over the growing season and the median RMSE is 7.16 μmol CO_2 m^{-2} s^{-1}, although the R^2 is high.

The use of a 15-day period for calculating the running mean is a compromise. In three of the sites analyzed, the highest median RMSE and the lowest median R^2 (Figure S5 in Supporting Information S2) is obtained for a shorter timescale (between three and seven days). After seven days the median R^2 increases for each site, except for FI-Hyy, which also shows a sharper downward trend in the bias error than the other cases. There are no significant changes in the computed metrics at timescale beyond 15 days, as the median RMSE and R^2 are rather constant at four out of five sites. Although among these sites there are some differences, in most of the cases these results suggest that the optimum timeframe for acclimation is between 10 and 30 days, where 15 days is an average timeframe across all five sites (Figure S5 in Supporting Information S2).

Comparison between observed and simulated GPP shows very little difference between the running mean and weighted mean approaches (Figure 4, Table 5). Visual comparison (Figure 4) indicates that the two approaches produce essentially identical estimates of GPP at BE-Vie, FI-Hyy, and GF-Guy. The median RMSE, R^2 and BE are slightly better for the weighted mean at BE-Vie, FI-Hyy, and GF-Guy than the running mean approach (Table 5). The weighted mean approach appears to produce marginally better results for the US-UMB site (R^2: 0.89), although both the median RMSE and BE are higher than those computed with the running mean, but a marginally worse estimate at the CH-Cha site (RMSE: 4.27 μmol CO_2 m^{-2} s^{-1}, Table 5).

19422466, 2022, 1, Downloaded from https://agupubs.onlinelibrary.wiley.com/doi/10.1029/2021MS002767 by Test, Wiley Online Library on [19/07/2024]. See the Terms and Conditions (https://onlinelibrary.wiley.com/terms-and-conditions) on Wiley Online Library for rules of use; OA articles are governed by the applicable Creative Commons License

19422466, 2022, 1, Downloaded from https://agupubs.onlinelibrary.wiley.com/doi/10.1029/2021MS002767 by Test, Wiley Online Library on [19/07/2024]. See the Terms and Conditions (https://onlinelibrary.wiley.com/terms-and-conditions) on Wiley Online Library for rules of use; OA articles are governed by the applicable Creative Commons License

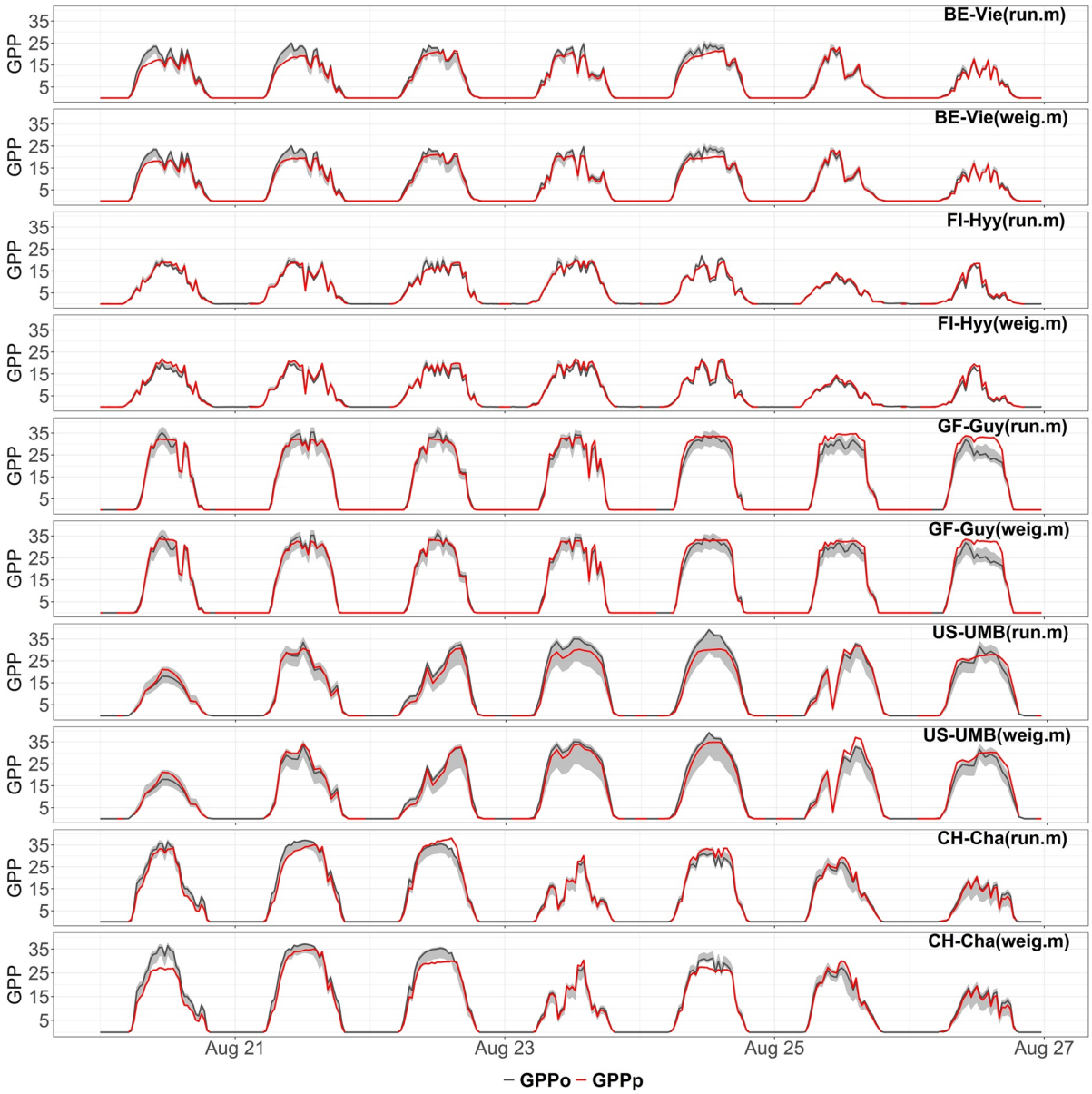

Figure 4. Comparison of the running mean (GPP_run.m) and weighted mean (GPP_weig.m) approaches for calculating gross primary production (GPP) for a single week in August 2014 at each of the five FLUXNET2015 sites. GPP is in units of μmol CO_2 m^{-2} s^{-1}. The gray shaded areas represent the uncertainty in GPPo calculated by the daytime partitioning method in the FLUXNET2015 data set.

Nevertheless, even for these two sites, the model performance using the weighted mean approach is consistent with the observed trends in the diurnal cycle. The R^2 values at the other sites (Table 5) are almost identical and although the RMSE suggested the running mean approach is better at four sites and worse at the fifth site, this is not consistent with the BE values.

The extended version of the P model, using the weighted mean approach, performs better overall than the CHTESSEL LSM. A visual comparison indicates that there is a better fit to the observed GPP at US-UMB and FI-Hyy (Figure 5) compared to the CHTESSEL simulations. The median R^2 over the growing season ranges from 0.88 to 0.98 for the P model compared to 0.68 to 0.91 for CHTESSEL (Table 6), and shows that the model performs better (sometimes substantially better) at every site. Comparing the range in the median RMSE between observed and predicted GPP from both models, there is a difference of about 1 μmol CO_2 m^{-2} s^{-1}. Model errors are also less for the P model than CHTESSEL, with the exception of the US-Syv site, where the P model overpredicts GPP

19422466, 2022, 1, Downloaded from https://agupubs.onlinelibrary.wiley.com/doi/10.1029/2021MS002767 by Test, Wiley Online Library on [19/07/2024]. See the Terms and Conditions (https://onlinelibrary.wiley.com/terms-and-conditions) on Wiley Online Library for rules of use; OA articles are governed by the applicable Creative Commons License

Table 5
Summary of Model Performance Statistics (RMSE Is the Root Mean Square Error, R^2 Is the Coefficient of Determination, and BE Is the Bias or Systematic Error) Using the Running Mean (Running) and Weighted Mean (Weighted) Methods Over the Growing Season at Each of the Sites

Site ID	Years	Median RMSE (running)	Median RMSE (weighted)	Median R^2 (running)	Median R^2 (weighted)	Median BE (running)	Median BE (weighted)
BE-Vie	2014	2.28	2.02	0.94	0.95	0.01	−0.003
FI-Hyy	2014	2.53	2.24	0.91	0.92	0.99	0.87
GF-Guy	2014	3.67	3.62	0.98	0.98	2.04	1.99
US-UMB	2014	3.54	3.75	0.88	0.89	1.98	2.02
CH-Cha	2014	3.89	4.27	0.88	0.90	1.07	0.67
DE-Gri	2014	2.12	2.30	0.97	0.97	−0.37	−0.39
RU-Fyo	2014	4.35	4.47	0.88	0.88	2.36	2.01
US-MMS	2014	4.25	4.01	0.95	0.94	2.01	1.96
US-Syv	2014	5.97	6.02	0.86	0.86	3.62	3.74
BR-Sa3	2003	5.31	5.63	0.91	0.92	1.43	−0.03

Note. These comparisons were made for 2014, except in the case of BR-Sa3 where data for 2014 were not available and an alternative year was used.

in 2006 substantially (median RMSE 12.11 μmol CO_2 m^{-2} s^{-1}) despite good observational coverage (98%) for this year. P model performance is better in summer (Figure 5, Figures S7, and S10 in Supporting Information S2) and autumn (Figures S8 and S11 in Supporting Information S2) than during the spring (Figures S6 and S9 in Supporting Information S2). There are differences between the vegetation type assigned in CHTESSEL and that present at some of these flux tower sites (e.g., US-UMB, see Table S4 in Supporting Information S2). However, this does not appear to explain the poorer overall performance of CHTESSEL, since the P model performs better both at these sites and sites with the correct vegetation type assigned (e.g., FI-Hyy). However, CHTESSEL captures the magnitude (though not necessarily the shape) of the diurnal variability during spring better than the P model at sites with cold winters (FI-Hyy, US-UMB, US-Syv, RU-Fyo, and US-MMS), where the P model tends to overestimate GPP.

4. Discussion

We have developed a version of the P model that predicts GPP at sub-daily timescales. This extended model reproduces well the diurnal cycle of GPP as recorded by flux-tower measurements across a range of different vegetation types. We have intentionally kept the model as simple as possible, as recommended for example, by Prentice et al. (2015), in the interests of clarity. The model has few parameters and their values are known from independent evidence. It does not distinguish between PFTs. We have succeeded in obtaining good simulations of flux data based on a minimal representation of the canopy as a big leaf. The complexity of the extended model (Figure 1) is only related to characteristics of the Farquhar et al. (1980) model itself, and those necessary to implement optimality hypotheses that have been extensively tested–see for example, Smith et al. (2019) for V_{cmax}, Wang et al. (2017) for χ and the ratio J_{max}:V_{cmax}.

We have shown that plants at these flux sites adjust to midday conditions rather than average daytime conditions. It is reasonable to expect that plants would optimize to conditions during the midday period, when the light is greatest (Haxeltine & Prentice, 1996; Maire et al., 2012; Smith et al., 2019). While this may be a good global approximation, we recognize that it may not be appropriate under some conditions. In dry areas, for example, plants effectively stop photosynthesizing in the warmest part of the day to minimize water loss and hydraulic damage. Midday depression in GPP, resulting from stomatal closure under high VPD, is characteristic of both crops and natural vegetation in dry areas (e.g., Pathre et al., 1998; Rambal et al., 2003; Wagle et al., 2015). Presumably, in such circumstances, plants may acclimate to early morning rather than midday conditions.

We have also shown that the timeframe for acclimation of carboxylation and electron-transport capacities, and the response of leaf-level carbon dioxide drawdown to vapor pressure deficit (VPD) is of the order of 15 days.

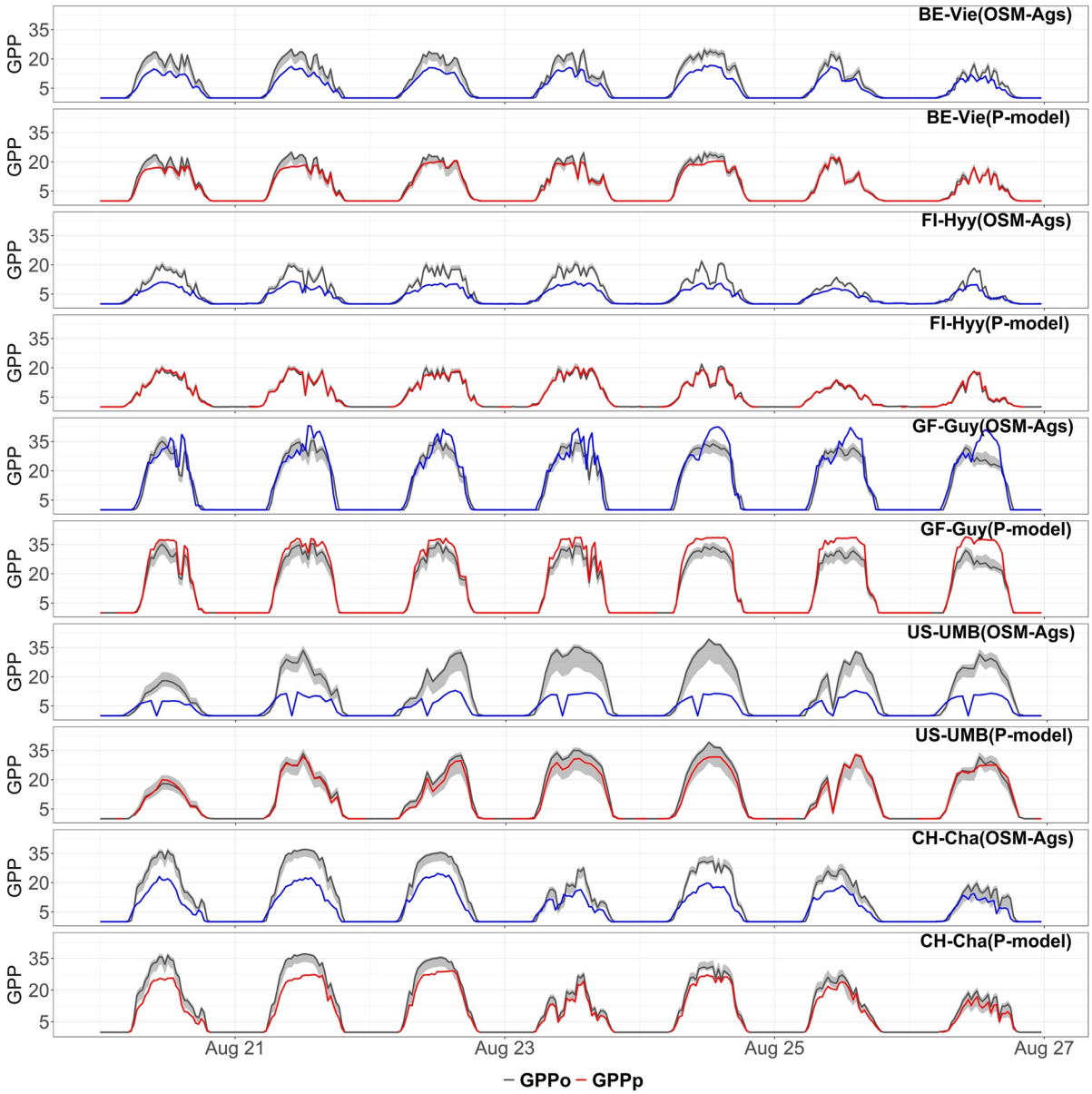

Figure 5. Comparison of simulated gross primary production by the P model (in red, labeled with site ID and "P-model") and by CHTESSEL (in blue, labeled with site ID and "OSM-Ags") and the GPP derived from eddy covariance flux-tower measurements (GPPo, in gray) for a single week in August 2014 at each of the five core FLUXNET2015 sites. GPP is in units of μmol CO_2 m^{-2} s^{-1}. The gray shaded areas represent the uncertainty in GPPo calculated by the daytime partitioning method in the FLUXNET2015 data set.

Accounting for environmental variations over longer time periods does not produce significant differences in model performance metrics. In the original version of the P model (Stocker et al., 2020; Wang et al., 2017), designed to simulate GPP at weekly to monthly time steps, these acclimated responses are implicit. Here they are explicit. Our analyses show that this distinction between fast and slow responses is essential to correctly predict plants' responses to the environment. However, we have not attempted to separate the acclimated timescales of carboxylation and electron-transport processes. While it is known that the Rubisco capacity acclimates to temperature over weeks, there is little evidence for the acclimation timescale of transport capacity.

The running mean and weighted averaging methods produce equally good simulations of the diurnal cycle of GPP. The weighted mean approach, using noon conditions as a timeframe, makes it possible to include acclimation in LSMs in a relatively straightforward way without having to specify PFT-specific parameters. Comparison

19422466, 2022, 1, Downloaded from https://agupubs.onlinelibrary.wiley.com/doi/10.1029/2021MS002767 by Test, Wiley Online Library on [19/07/2024]. See the Terms and Conditions (https://onlinelibrary.wiley.com/terms-and-conditions) on Wiley Online Library for rules of use; OA articles are governed by the applicable Creative Commons License

19422466, 2022, 1, Downloaded from https://agupubs.onlinelibrary.wiley.com/doi/10.1029/2021MS002767 by Test, Wiley Online Library on [19/07/2024]. See the Terms and Conditions (https://onlinelibrary.wiley.com/terms-and-conditions) on Wiley Online Library for rules of use; OA articles are governed by the applicable Creative Commons License

Table 6
Summary of the Two Models' Performance Statistics (Root-Mean Square Error is the Root Mean Square Error, R^2 Is the Coefficient of Determination, and BE Is the Bias or Systematic error) Over the Growing Season at Each of the Sites. These Comparisons Were Made for 2014, Except in the Case of BR-Sa3 and US-Syv Where Data for 2014 Were Not Available and an Alternative Year Was Used

Site ID	Years	Median RMSE P model	Median RMSE CHTESSEL	Median R^2 P model	Median R^2 CHTESSEL	Median BE P model	Median BE CHTESSEL
BE-Vie	2014	1.73	3.19	0.95	0.89	−0.02	−1.52
FI-Hyy	2014	2.21	2.85	0.92	0.81	1.07	−1.06
GF-Guy	2014	3.8	4.10	0.98	0.91	2.14	0.95
US-UMB	2014	3.53	4.81	0.88	0.68	1.19	−1.65
CH-Cha	2014	4.3	5.20	0.9	0.89	−1.83	−2.12
DE-Gri	2014	3.49	5.49	0.97	0.89	−1.49	−2.78
RU-Fyo	2014	2.66	2.86	0.89	0.84	1.26	−1.46
US-MMS	2014	4.04	6.51	0.95	0.72	1.93	−2.52
US-Syv	2006	12.11	2.32	0.94	0.86	7.71	−0.46
BR-Sa3	2003	6.13	8.33	0.92	0.86	−1.60	−4.76

shows that the extended version of the P model using the weighted mean approach provides better estimates of GPP than CHTESSEL at most sites and for most years analyzed. LSMs have to specify different values of V_{cmax25} and J_{max25} for plants growing in different environments, as represented by PFTs, precisely because they do not represent acclimation. Moreover, the need to specify PFTs creates uncertainty in model evaluations, as shown here (Figure 5) for a number of cases where the PFT assignments in the operational model do not match the actual PFT at the flux sites. As our results show, simulation would be more accurate, as well as requiring fewer parameters, if acclimation were allowed universally (in time and space) – so accounting more realistically both for seasonal variation, and presumably also representing the responses to environmental change better.

We have adapted the P model to work at a half-hourly timescale, as the model has previously been tested at monthly and weekly timescales only. The method proposed here has succeeded in representing sub-daily as well as seasonal dynamics of GPP in different biomes with no need for site- or PFT-specific calibration. However, some issues still need to be addressed. There is a tendency for the model to overpredict GPP in spring compared to CHTESSEL at some sites, particularly those where the winters are cold. This is a known issue (Stocker et al., 2020) and suggests that the P model does not account properly for the time required to adjust to cold conditions at the start of the growing season. Similarly, the P model (in common with many LSMs), tends to overpredict GPP in very dry areas because the model does not account for the effect of low soil moisture (as opposed to atmospheric dryness) on photosynthesis (Stocker et al., 2020). Combining the VPD response and the response to soil moisture at sub-daily timescale is a challenge that needs to be addressed before the model can be applied globally.

5. Conclusions

We have adapted an existing optimality-based modeling framework to operate successfully at sub-daily timescale. The P model, without PFT-dependent photosynthetic parameters, accurately predicts GPP at half-hourly timestep across a range of different biomes. The method we propose is able to manage both timescales of acclimation. The weighted mean approach is suitable for implementation in an LSM. Our results suggest a way forward for LSMs to reduce their dependence on multiple parameters while, at the same time, taking into account plants' acclimation to the environment.

19422466, 2022, 1, Downloaded from https://agupubs.onlinelibrary.wiley.com/doi/10.1029/2021MS002767 by Test, Wiley Online Library on [19/07/2024]. See the Terms and Conditions (https://onlinelibrary.wiley.com/terms-and-conditions) on Wiley Online Library for rules of use; OA articles are governed by the applicable Creative Commons License

Data Availability Statement

The half-hourly implementation of the P model is generated with RStudio and is available through GitHub public repository: https://github.com/GiuliaMengoli/P-model_subDaily. Data sets for this research are available in these in-text data citation references: Pastorello et al. (2020), [Creative Commons (CC-BY 4.0) license], Stocker 2020, [http://doi.org/10.5281/zenodo.4392703]; The LAI used in this study is available under (https://github.com/GiuliaMengoli/P-model_subDaily/tree/main/LAI_data). It is based on MODIS collection 5 (Myneni et al., 2002) and adapted to fit the CHTESSEL configuration by Boussetta, Balsamo, Beljaars, Kral, and Jarlan (2013).

Acknowledgments
GM and ICP acknowledge support from the ERC-funded project REALM (grant number 787203). SPH acknowledges support from the ERC-funded project GC2.0 (Global Change 2.0: Unlocking the past for a clearer future, grant number 694481). GM acknowledges Gianpaolo Balsamo and Gabriele Arduini for useful discussions and technical assistance at the ECMWF centre. GM acknowledges Benjamin D. Stocker for providing fAPAR data. We thank Martin De Kauwe and Marc Peaucelle for helpful comments on an earlier version of the manuscript.

References

Anav, A., Friedlingstein, P., Beer, C., Ciais, P., Harper, A., Jones, C., et al. (2015). Spatiotemporal patterns of terrestrial gross primary production: A review. *Reviews of Geophysics*, *53*(3), 785–818. https://doi.org/10.1002/2015RG000483

Anav, A., Friedlingstein, P., Kidston, M., Bopp, L., Ciais, P., Cox, P., et al. (2013). Evaluating the land and ocean Components of the global carbon cycle in the CMIP5 Earth System Models. *Journal of Climate*, *26*(18), 6801–6843. https://doi.org/10.1175/JCLI-D-12-00417.1

Atkin, O. K., Atkinson, L. J., Fisher, R. A., Campbell, C. D., Zaragoza-Castells, J., Pitchford, J. W., et al. (2008). Using temperature-dependent changes in leaf scaling relationships to quantitatively account for thermal acclimation of respiration in a coupled global climate–vegetation model. *Global Change Biology*, *14*(11), 2709–2726. https://doi.org/10.1111/j.1365-2486.2008.01664.x

Balsamo, G., Beljaars, A., Scipal, K., Viterbo, P., van den Hurk, B., Hirschi, M., & Betts, A. K. (2009). A revised hydrology for the ECMWF Model: Verification from field site to terrestrial water storage and impact in the Integrated Forecast System. *Journal of Hydrometeorology*, *10*(3), 623–643. https://doi.org/10.1175/2008JHM1068.1

Berberan-Santos, M. N., Bodunov, E. N., & Pogliani, L. (1997). On the barometric formula. *American Journal of Physics*, *65*(5), 404–412. https://doi.org/10.1119/1.18555

Bernacchi, C. J., Pimentel, C., & Long, S. P. (2003). In vivo temperature response functions of parameters required to model RuBP-limited photosynthesis. *Plant, Cell & Environment*, *26*(9), 1419–1430. https://doi.org/10.1046/j.0016-8025.2003.01050.x

Bernacchi, C. J., Singsaas, E. L., Pimentel, C., Portis, A. R., Jr, & Long, S. P. (2001). Improved temperature response functions for models of Rubisco-limited photosynthesis. *Plant, Cell & Environment*, *24*(2), 253–259. https://doi.org/10.1111/j.1365-3040.2001.00668.x

Bloomfield, K. J., Prentice, I. C., Cernusak, L. A., Eamus, D., Medlyn, B. E., Rumman, R., et al. (2019). The validity of optimal leaf traits modelled on environmental conditions. *New Phytologist*, *221*(3), 1409–1423. https://doi.org/10.1111/nph.15495

Bonan, G., Pollard, D., & Thompson, S. (1992). Effects of boreal forest vegetation on global climate. *Nature*, *359*, 716–718. https://doi.org/10.1038/359716a0

Bonan, G. B. (2008). Forests and climate change: Forcings, feedbacks, and the climate benefits of forests. *Science*, *320*(5882), 1444–1449. https://doi.org/10.1126/science.1155121

Bonan, G. B., Levis, S., Sitch, S., Vertenstein, M., & Oleson, K. W. (2003). A dynamic global vegetation model for use with climate models: Concepts and description of simulated vegetation dynamics. *Global Change Biology*, *9*(11), 1543–1566. https://doi.org/10.1046/j.1365-2486.2003.00681.x

Boussetta, S., Balsamo, G., Beljaars, A., Kral, T., & Jarlan, L. (2013). Impact of a satellite-derived leaf area index monthly climatology in a global numerical weather prediction model. *International Journal of Remote Sensing*, *34*(9–10), 3520–3542. https://doi.org/10.1080/01431161.2012.716543

Boussetta, S., Balsamo, G., Beljaars, A., Panareda, A.-A., Calvet, J.-C., Jacobs, C., et al. (2013). Natural land carbon dioxide exchanges in the ECMWF integrated forecasting system: Implementation and offline validation. *Journal of Geophysical Research: Atmospheres*, *118*(12), 5923–5946. https://doi.org/10.1002/jgrd.50488

Campos de Oliveira, M. H., Sari, V., dos Reis Castro, N. M., & Pedrollo, O. C. (2017). Estimation of soil water content in watershed using artificial neural networks. *Hydrological Sciences Journal*, *62*(13), 2120–2138. https://doi.org/10.1080/02626667.2017.1364844

Ciais, P., Sabine, C., Bala, G., Bopp, L., Brovkin, V., & Canadell, J. (2013). Carbon and other biogeochemical cycles. In C. Heinze, P. Tans, & T. Vesala (Eds.), *Climate change 2013: The physical science basis. Contribution of working group I to the fifth assessment report of the intergovernmental panel on climate change* (pp. 465–570). Cambridge University Press. https://www.ipcc.ch/site/assets/uploads/2018/02/WG1AR5_Chapter06_FINAL.pdf

Dong, N., Prentice, I. C., Wright, I. J., Evans, B. J., Togashi, H. F., Caddy-Retalic, S., et al. (2020). Components of leaf-trait variation along environmental gradients. *New Phytologist*, *228*, 82–94. https://doi.org/10.1111/nph.16558

Farquhar, G. D., von Caemmerer, S., & Berry, J. A. (1980). A biochemical model of photosynthetic CO_2 assimilation in leaves of C3 species. *Planta*, *149*(1), 78–90. https://doi.org/10.1007/BF00386231

Fisher, R. A., & Koven, C. D. (2020). Perspectives on the future of land surface models and the challenges of representing complex terrestrial systems. *Journal of Advances in Modeling Earth Systems*, *12*(4), e2018MS001453. https://doi.org/10.1029/2018ms001453

Franklin, O., Harrison, S. P., Dewar, R., Farrior, C. E., Brannstrom, A., Dieckmann, U., et al. (2020). Organizing principles for vegetation dynamics. *Nature Plants*, *6*(5), 444–453. https://doi.org/10.1038/s41477-020-0655-x

Harrison, S. P., Cramer, W., Franklin, O., Prentice, I. C., Wang, H., Brännström, Å., et al. (2021). Eco-evolutionary optimality as a means to improve vegetation and land-surface models. *New Phytologist*, *231*, 2125–2141. https://doi.org/10.1111/nph.17558

Haxeltine, A., & Prentice, I. C. (1996). A general model for the light-use efficiency of primary production. *Functional Ecology*, *10*(5), 551–561. https://doi.org/10.2307/2390165

Huber, M. L., Perkins, R. A., Laesecke, A., Friend, D. G., Sengers, J. V., Assael, M. J., et al. (2009). New international formulation for the viscosity of H_2O. *Journal of Physical and Chemical Reference Data*, *38*(2), 101–125. https://doi.org/10.1063/1.3088050

Jacobs, C. M. J. (1994). *Direct impact of atmospheric CO_2 enrichment on regional transpiration*. In S. l. Jacobs (Ed.). Retrieved from https://edepot.wur.nl/206972

Jacobs, C. M. J., van den Hurk, B. M. M., & de Bruin, H. A. R. (1996). Stomatal behaviour and photosynthetic rate of unstressed grapevines in semi-arid conditions. *Agricultural and Forest Meteorology*, *80*(2), 111–134. https://doi.org/10.1016/0168-1923(95)02295-3

Kattge, J., & Knorr, W. (2007). Temperature acclimation in a biochemical model of photosynthesis: A reanalysis of data from 36 species. *Plant, Cell & Environment*, *30*(9), 1176–1190. https://doi.org/10.1111/j.1365-3040.2007.01690.x

Lasslop, G., Migliavacca, M., Bohrer, G., Reichstein, M., Bahn, M., Ibrom, A., et al. (2012). On the choice of the driving temperature for eddy-covariance carbon dioxide flux partitioning. *Biogeosciences*, *9*(12), 5243–5259. https://doi.org/10.5194/bg-9-5243-2012

Lasslop, G., Reichstein, M., Papale, D., Richardson, A. D., Arneth, A., Barr, A., et al. (2010). Separation of net ecosystem exchange into assimilation and respiration using a light response curve approach: Critical issues and global evaluation. *Global Change Biology*, *16*(1), 187–208. https://doi.org/10.1111/j.1365-2486.2009.02041.x

Lawrence, D. M., Fisher, R. A., Koven, C. D., Oleson, K. W., Swenson, S. C., Bonan, G., et al. (2019). The community land model version 5: Description of new features, benchmarking, and impact of forcing uncertainty. *Journal of Advances in Modeling Earth Systems*, *11*(12), 4245–4287. https://doi.org/10.1029/2018ms001583

Lin, Y.-S., Medlyn, B. E., Duursma, R. A., Prentice, I. C., Wang, H., Baig, S., et al. (2015). Optimal stomatal behaviour around the world. *Nature Climate Change*, *5*(5), 459–464. https://doi.org/10.1038/nclimate2550

Lombardozzi, D. L., Bonan, G. B., Smith, N. G., Dukes, J. S., & Fisher, R. A. (2015). Temperature acclimation of photosynthesis and respiration: A key uncertainty in the carbon cycle-climate feedback. *Geophysical Research Letters*, *42*(20), 8624–8631. https://doi.org/10.1002/2015gl065934

Luo, X., & Keenan, T. F. (2020). Global evidence for the acclimation of ecosystem photosynthesis to light. *Nature Ecology & Evolution*, *4*(10), 1351–1357. https://doi.org/10.1038/s41559-020-1258-7

Maire, V., Martre, P., Kattge, J., Gastal, F., Esser, G., Fontaine, S., & Soussana, J.-F. (2012). The coordination of leaf photosynthesis links C and N fluxes in C_3 plant species. *PLoS One*, *7*(6), e38345. https://doi.org/10.1371/journal.pone.0038345

Mäkelä, J., Knauer, J., Aurela, M., Black, A., Heimann, M., Kobayashi, H., et al. (2019). Land surface model photosynthesis and parameter calibration for boreal sites with adaptive population importance sampler. *Geoscientific Model Development*, *12*, 4075–4098. https://doi.org/10.5194/gmd-2018-313

Marchin, R. M., Broadhead, A. A., Bostic, L. E., Dunn, R. R., & Hoffmann, W. A. (2016). Stomatal acclimation to vapour pressure deficit doubles transpiration of small tree seedlings with warming. *Plant, Cell & Environment*, *39*(10), 2221–2234. https://doi.org/10.1111/pce.12790

Medlyn, B. E., Duursma, R. A., Eamus, D., Ellsworth, D. S., Prentice, I. C., Barton, C. V. M., et al. (2011). Reconciling the optimal and empirical approaches to modelling stomatal conductance. *Global Change Biology*, *17*(6), 2134–2144. https://doi.org/10.1111/j.1365-2486.2010.02375.x

Meir, P., Kruijt, B., Broadmeadow, M., Barbosa, E., Kull, O., Carswell, F., et al. (2002). Acclimation of photosynthetic capacity to irradiance in tree canopies in relation to leaf nitrogen concentration and leaf mass per unit area. *Plant, Cell & Environment*, *25*(3), 343–357. https://doi.org/10.1046/j.0016-8025.2001.00811.x

Myneni, R., Hoffman, S., knyazikhin, Y., Privette, J., Glassy, J., Tian, Y., et. al. (2002). Global products of vegetation leaf area and fraction absorbed PAR from year one of MODIS data. *Remote Sensing of Environment*, *83*(1–2), 214–231. https://doi.org/10.1016/S0034-4257(02)00074-3

Myneni, R., Knyazikhin, Y., & Park, T. (2015). MCD15A3H MODIS/Terra+Aqua Leaf Area Index/FPAR 4-day L4 Global 500m SIN Grid V006[Data set]. NASA EOSDIS Land Processes DAAC. https://doi.org/10.5067/MODIS/MCD15A3H.006

Pastorello, G., Trotta, C., Canfora, E., Chu, H., Christianson, D., Cheah, Y. W., et al. (2020). The FLUXNET2015 dataset and the ONEFlux processing pipeline for eddy covariance data. *Scientific Data*, *7*(1), 225. https://doi.org/10.1038/s41597-020-0534-3

Pathre, U., Sinha, A. K., Shirke, P. A., & Sane, P. V. (1998). Factors determining the midday depression of photosynthesis in trees under monsoon climate. *Trees*, *12*, 472–481. https://doi.org/10.1007/s004680050177

Prentice, I. C., & Cowling, S. A. (2013). Dynamic Global Vegetation Models. In *Encyclopedia of biodiversity* (pp. 670–689). https://doi.org/10.1016/b978-0-12-384719-5.00412-3

Prentice, I. C., Dong, N., Gleason, S. M., Maire, V., & Wright, I. J. (2014). Balancing the costs of carbon gain and water transport: Testing a new theoretical framework for plant functional ecology. *Ecology Letters*, *17*(1), 82–91. https://doi.org/10.1111/ele.12211

Prentice, I. C., Liang, X., Medlyn, B. E., & Wang, Y. P. (2015). Reliable, robust and realistic: The three R's of next-generation land-surface modelling. *Atmopheric Chemistry and Physics*, *15*(10), 5987–6005. https://doi.org/10.5194/acp-15-5987-2015

Qiao, S., Wang, H., Prentice, I. C., & Harrison, S. P. (2020). Extending a first-principles primary production model to predict wheat yields. *Agricultural and Forest Meteorology*, *287*. https://doi.org/10.1016/j.agrformet.2020.107932

Rambal, S., Ourcival, J.-M., Joffre, R., Mouillot, F., Nouvellon, Y., Reichstein, M., & Rocheteau, A. (2003). Drought controls over conductance and assimilation of a Mediterranean evergreen ecosystem: Scaling from leaf to canopy. *Global Change Biology*, *9*(12), 1813–1824. https://doi.org/10.1111/j.1365-2486.2003.00687.x

Rogers, A., Medlyn, B. E., Dukes, J. S., Bonan, G., von Caemmerer, S., Dietze, M. C., et al. (2017). A roadmap for improving the representation of photosynthesis in Earth system models. *New Phytologist*, *213*(1), 22–42. https://doi.org/10.1111/nph.14283

Rogers, A., Serbin, S. P., Ely, K. S., & Wullschleger, S. D. (2019). Terrestrial biosphere models may overestimate Arctic CO_2 assimilation if they do not account for decreased quantum yield and convexity at low temperature. *New Phytologist*, *223*(1), 167–179. https://doi.org/10.1111/nph.15750

Singsaas, E. L., Ort, D. R., & DeLucia, E. H. (2001). Variation in measured values of photosynthetic quantum yield in ecophysiological studies. *Oecologia*, *128*(1), 15–23. https://doi.org/10.1007/s004420000624

Smith, E. L. (1937). The influence of light and carbon dioxide on photosynthesis. *The Journal of General Physiology*, *20*(6), 807–830. https://doi.org/10.1085/jgp.20.6.807

Smith, N. G., & Dukes, J. S. (2013). Plant respiration and photosynthesis in global-scale models: Incorporating acclimation to temperature and CO_2. *Global Change Biology*, *19*(1), 45–63. https://doi.org/10.1111/j.1365-2486.2012.02797.x

Smith, N. G., Keenan, T. F., Colin Prentice, I., Wang, H., Wright, I. J., Niinemets, U., et al. (2019). Global photosynthetic capacity is optimized to the environment. *Ecology Letters*, *22*(3), 506–517. https://doi.org/10.1111/ele.13210

Smith, N. G., Lombardozzi, D., Tawfik, A., Bonan, G., & Dukes, J. S. (2017). Biophysical consequences of photosynthetic temperature acclimation for climate. *Journal of Advances in Modeling Earth Systems*, *9*(1), 536–547. https://doi.org/10.1002/2016ms000732

Stocker, B. (2020). stineb/ingestr: Dummy release for Zenodo (Version v1.1). *Zenodo*. https://doi.org/10.5281/zenodo.4392703

Stocker, B. D., Wang, H., Smith, N. G., Harrison, S. P., Keenan, T. F., Sandoval, D., et al. (2020). P-model v1.0: An optimality-based light use efficiency model for simulating ecosystem gross primary production. *Geoscientific Model Development*, *13*(3), 1545–1581. https://doi.org/10.5194/gmd-13-1545-2020

Togashi, H. F., Prentice, I. C., Atkin, O. K., Macfarlane, C., Prober, S. M., Bloomfield, K. J., & Evans, B. J. (2018). Thermal acclimation of leaf photosynthetic traits in an evergreen woodland, consistent with the coordination hypothesis. *Biogeosciences*, *15*(11), 3461–3474. https://doi.org/10.5194/bg-15-3461-2018

Vanderwel, M. C., Slot, M., Lichstein, J. W., Reich, P. B., Kattge, J., Atkin, O. K., et al. (2015). Global convergence in leaf respiration from estimates of thermal acclimation across time and space. *New Phytologist*, *207*(4), 1026–1037. https://doi.org/10.1111/nph.13417

Viterbo, P., Beljaars, A., Mahfouf, J.-F., & Teixeira, J. (1999). The representation of soil moisture freezing and its impact on the stable boundary layer. *Quarterly Journal of the Royal Meteorological Society*, *125*(559), 2401–2426. https://doi.org/10.1002/qj.49712555904

19422466, 2022, 1, Downloaded from https://agupubs.onlinelibrary.wiley.com/doi/10.1029/2021MS002767 by Test, Wiley Online Library on [19/07/2024]. See the Terms and Conditions (https://onlinelibrary.wiley.com/terms-and-conditions) on Wiley Online Library for rules of use; OA articles are governed by the applicable Creative Commons License

Wagle, P., Xiao, X., & Suyker, A. E. (2015). Estimation and analysis of gross primary production of soybean under various management practices and drought conditions. *ISPRS Journal of Photogrammetry and Remote Sensing*, *99*, 70–83. https://doi.org/10.1016/j.isprsjprs.2014.10.009

Walker, A. P., Quaife, T., van Bodegom, P. M., De Kauwe, M. G., Keenan, T. F., Joiner, J., et al. (2017). The impact of alternative trait-scaling hypotheses for the maximum photosynthetic carboxylation rate (Vcmax) on global gross primary production. *New Phytologist*, *215*(4), 1370–1386. https://doi.org/10.1111/nph.14623

Wang, H., Atkin, O. K., Keenan, T. F., Smith, N. G., Wright, I. J., Bloomfield, K. J., et al. (2020). Acclimation of leaf respiration consistent with optimal photosynthetic capacity. *Global Change Biology*, *26*(4), 2573–2583. https://doi.org/10.1111/gcb.14980

Wang, H., Prentice, I. C., Keenan, T. F., Davis, T. W., Wright, I. J., Cornwell, W. K., et al. (2017). Towards a universal model for carbon dioxide uptake by plants. *Nature Plants*, *3*(9), 734–741. https://doi.org/10.1038/s41477-017-0006-8

Yu, J., Kim, S. B., Bai, J., & Han, S. W. (2020). Comparative study on exponentially weighted moving average approaches for the self-starting forecasting. *Applied Sciences*, *10*(20). https://doi.org/10.3390/app10207351

Zhang, Y., Kong, D., Gan, R., Chiew, F. H. S., McVicar, T. R., Zhang, Q., & Yang, Y. (2019). Coupled estimation of 500 m and 8-day resolution global evapotranspiration and gross primary production in 2002–2017. *Remote Sensing of Environment*, *222*, 165–182. https://doi.org/10.1016/j.rse.2018.12.031

19422466, 2022, 1, Downloaded from https://agupubs.onlinelibrary.wiley.com/doi/10.1029/2021MS002767 by Test, Wiley Online Library on [19/07/2024]. See the Terms and Conditions (https://onlinelibrary.wiley.com/terms-and-conditions) on Wiley Online Library for rules of use; OA articles are governed by the applicable Creative Commons License